

## Particle decays from $^{12}\text{B}$ and $^{12}\text{N}$ mirror nuclei

T. Inomata,<sup>1</sup> H. Akimune,<sup>1</sup> I. Daito,<sup>1</sup> H. Ejiri,<sup>1</sup> H. Fujimura,<sup>1</sup> Y. Fujita,<sup>2</sup> M. Fujiwara,<sup>1</sup> M. N. Harakeh,<sup>3</sup> K. Ishibashi,<sup>1</sup> H. Kohri,<sup>1</sup> N. Matsuoka,<sup>1</sup> S. Nakayama,<sup>4</sup> A. Tamii,<sup>5</sup> M. Tanaka,<sup>6</sup> H. Toyokawa,<sup>7</sup> M. Yoshimura,<sup>1</sup> and M. Yosoi<sup>5</sup>

<sup>1</sup>Research Center for Nuclear Physics, Osaka University, Ibaraki, Osaka 567, Japan

<sup>2</sup>Department of Physics, Osaka University, Toyonaka, Osaka 560, Japan

<sup>3</sup>Kernfysisch Versneller Instituut, Zernikelaan 25, 9747 AA Groningen, The Netherlands

<sup>4</sup>Department of Physics, Tokushima University, Tokushima, Japan

<sup>5</sup>Department of Physics, Kyoto University, Sakyo-ku, Kyoto 606-01, Japan

<sup>6</sup>Kobe Tokiwa Jr. College, Nagataku, Kobe 653, Japan

<sup>7</sup>SPRING-8, Kamigori-cho, Ako-gun, Hyogo 678-12, Japan

(Received 22 December 1997)

Spin-isospin excitations in  $^{12}\text{B}$  and  $^{12}\text{N}$  have been studied using the  $^{12}\text{C}(d,^2\text{He})^{12}\text{B}$  and  $^{12}\text{C}(^3\text{He},t)^{12}\text{N}$  charge-exchange reactions at  $\theta = 0^\circ$  and at  $E_d=200$  MeV and  $E(^3\text{He})=450$  MeV, respectively. Neutron decay from  $^{12}\text{B}$  to  $^{11}\text{B}$  and proton decay from  $^{12}\text{N}$  to  $^{11}\text{C}$  have been measured with detector arrays consisting of liquid-scintillation counters and silicon detectors, respectively. Microscopic structures of the spin-dipole resonances in  $^{12}\text{B}$  and  $^{12}\text{N}$  are discussed on the basis of the experimental observations of particle decays and their angular correlations. [S0556-2813(98)02606-5]

PACS number(s): 24.30.Cz, 25.55.Kr, 27.20.+n, 29.30.Aj

### I. INTRODUCTION

Giant resonances in nuclei are coherent vibrations of nucleons moving in a restoring nuclear potential. They are characterized by quantum numbers, spin and parity  $J^\pi$ . They are observed as broad peaks in the excitation-energy region from several MeV to tens of MeV. Particular examples are the spin-isospin resonances, such as the Gamow-Teller resonances (GTR's) [1,2], which are strongly excited via the charge-exchange reactions at intermediate energies. The GTR's are mediated by the  $\vec{\sigma} \cdot \vec{\tau}$  operator.

Spin-dipole resonances (SDR's) mediated by the  $\vec{\sigma} \cdot \vec{\tau} Y_1$  operator have been observed in  $(p,n)$  reactions [3–6], as well as in  $(^3\text{He},t)$  reactions [7]. The angular distributions obtained in the charge-exchange reactions leading to SDR's have characteristic  $\Delta L=1$  shapes. Dipole excitations observed in charge-exchange reactions at bombarding energies of  $\leq 60$  MeV/nucleon have been associated with the giant dipole resonance (GDR) mediated with the operator  $\vec{\tau} r Y_1$ . Tabor *et al.* gave [8] an overview of spectra obtained with the  $(^3\text{He},t)$  reactions at 130 and 170 MeV on various nuclei ranging from  $^{12}\text{C}$  to  $^{90}\text{Zr}$ . They found that in all cases the broad bumps standing on the nuclear continuum are located at nearly the same excitation energies and have similar widths as those of the GDR excited in the photonuclear reaction [9]. Although the observed bumps have been associated with the GDR at low bombarding energies in charge-exchange reactions where spin transfer can be involved, the transferred orbital angular momentum of  $\Delta L=1$  can, in principle, couple to a spin transfer  $\Delta S=1$ , resulting in a transferred total angular momentum  $\Delta J^\pi=0^-, 1^-,$  and  $2^-$ . Ejiri, Ikeda, and Fujita [10,11] predicted the existence of these giant resonances with  $\Delta L=1$ ,  $\Delta S=1$ ,  $\Delta T=1$  by analyzing the data of  $E1$  transitions from the analog states and  $M2$  transitions in medium-heavy nuclei [10].

Isovector  $0^+ \rightarrow 0^-$  transitions are of special interest since

the process includes the same quantum numbers  $0^-$  as the  $\pi$  mesons which, therefore, play a very important role in these transitions. Because of this reason, the  $0^- \rightarrow 0^+$   $\beta$  decays and the  $0^+ \rightarrow 0^-$  transitions in charge-exchange reactions were repeatedly studied theoretically [12,13]. If the transitions to  $0^-$  states can be separated from transitions to the other states in the SDR, one can test the effect of the pion field in nuclei using charge-exchange reactions. Unfortunately, until now, no successful extraction of the  $0^-$  component from the complex mixture of the  $0^-$ ,  $1^-$ , and  $2^-$  states in the SDR has been reported since these states overlap strongly with each other and are populated with the same transferred orbital angular momentum  $\Delta L=1$ .

Typical candidates of these  $0^-$ ,  $1^-$ , and  $2^-$  states are expected in the  $A=12$  mirror nuclei of  $^{12}\text{B}$  and  $^{12}\text{N}$ . Figure 1 shows the spin-isospin excitation modes in the  $A=12$  nuclei and their decay schemes [14]. The proton separation energy ( $S_p$ ) of  $^{12}\text{B}$  and the neutron separation energy ( $S_n$ ) of  $^{12}\text{N}$  are 14.1 and 15.7 MeV, respectively. On the other hand, the neutron separation energy ( $S_n$ ) of  $^{12}\text{B}$  and the proton separation energy ( $S_p$ ) of  $^{12}\text{N}$  are 3.4 and 0.6 MeV, respectively. Thus, only the mirror particle decay modes from the spin-dipole resonances in  $^{12}\text{B}$  and  $^{12}\text{N}$  are allowed, i.e., neutron decay of  $^{12}\text{B}$  and proton decay of  $^{12}\text{N}$ .

The charge-exchange reactions on  $^{12}\text{C}$  at intermediate energies lead to several prominent peaks in the spectra. They are the  $1^+$  ground state, the  $2^-$  spin-dipole state at  $\sim 4$  MeV, and  $1^-$  dipole and spin-dipole resonances around 7 MeV. A  $0^-$  state expected at  $\sim 9$  MeV has never been clearly identified experimentally.

There are two recent  $(p,n)$  results [15,16], in which the 7 MeV peak in  $^{12}\text{N}$  is well described with the  $1^-$  assumption, consisting with the theoretical prediction. However, there is a contradicting conclusion concerning the presence of the  $1^-$  state at  $\sim 7$  MeV in  $^{12}\text{B}$  from the tensor-analyzing-power measurement of the  $(d,^2\text{He})$  reaction at 270 MeV [17,18].

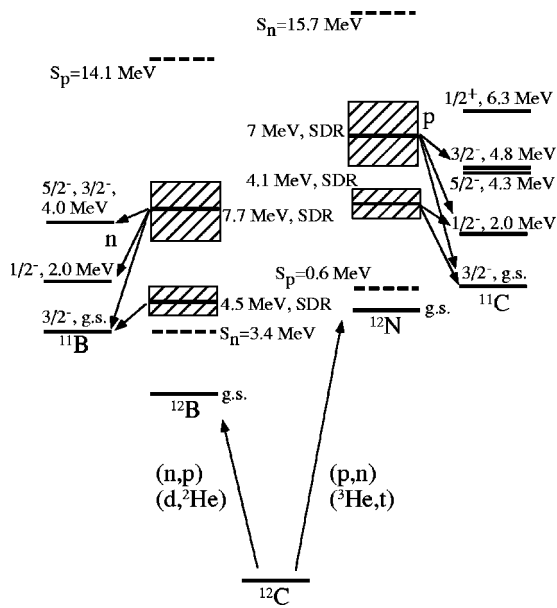


FIG. 1. Level schemes of  $^{12}\text{B}$  and  $^{12}\text{N}$ . The particle threshold energies are indicated for proton and neutron decays.

Okamura *et al.* [17,18] suggested that the tensor-analyzing power of the  $^{12}\text{C}(d, ^2\text{He})^{12}\text{B}$  reaction for the 7 MeV resonance is better described with the  $2^-$  assumption despite the  $1^-$  theoretical prediction. Thus, the conclusion about the spin-parity assignment for the 7 MeV resonance of the SDR is still controversial. A more exclusive independent measurement, which differs from the simple measurements of cross sections and analyzing powers, will be very useful in resolving this problem.

The angular correlation for decay particles from states excited in a charge-exchange reaction is believed to be a powerful means to provide precious information on the nuclear structure of the intermediate and final states and on the  $J^\pi$  values of the intermediate state. In order to perform the present measurements, we use two independent charge-exchange reactions,  $^{12}\text{C}(d, ^2\text{He})$  and  $^{12}\text{C}(^3\text{He}, t)$ , leading to the final mirror nuclei  $^{12}\text{B}$  and  $^{12}\text{N}$ , respectively.

The  $(d, ^2\text{He})$  reaction is the most powerful probe among various possible reactions to excite the spin-isospin modes of the  $\Delta T_z = +1$  channel, where the  $^2\text{He}$  particle is observed as a pair of protons coupled to the unbound  $^1S_0$  ( $T=1$ ) state [19]. This reaction picks up only the  $\Delta S=1$  components, and thus no spin-flip measurement is required to sort out the  $\Delta S=0$  and 1 components. With the advantage of its unique selectivity ( $\Delta S=1$ ,  $\Delta T=1$ , and  $\Delta T_z = +1$ ), the  $(d, ^2\text{He})$  reaction becomes a good tool for studying Gamow-Teller and spin-flip dipole transitions [17,18,20–22] although the experiment and its data analyses are rather difficult. It is noteworthy to mention that another interesting probe is the  $(^7\text{Li}, ^7\text{Be})$  reaction, which makes it possible to discriminate between the  $\Delta S=0$  and  $\Delta S=1$  spectra by measuring the transitions to the ground state and the first-excited state in  $^7\text{Be}$  under similar kinematical conditions [23–25]. The transitions to the first-excited state are identified by measuring the  $^7\text{Be}$  ejectiles in coincidence with decay  $\gamma$  rays from the first-excited state in  $^7\text{Be}$ .

We succeeded in measuring the  $^2\text{He}$  particles in coincidence with decay neutrons. This is, indeed, a triple-

coincidence experiment. The two protons constituting the  $^2\text{He}$  particle must be measured in coincidence under the intense proton background originating from the deuteron breakup reaction at forward angles. Furthermore, detection of neutral neutrons in coincidence with  $^2\text{He}$  particles makes the experiment more difficult. The threshold energy for neutron decay in  $^{12}\text{B}$  is 3.4 MeV (see Fig. 1) [14], while the proton decay threshold is 14.1 MeV. Thus, it is possible to measure decay neutrons from the levels at  $E_x = 3.4 \sim 14.1$  MeV in  $^{12}\text{B}$ .

The first  $(^3\text{He}, t + p)$  coincidence measurements have been performed at energies of  $\sim 30$  MeV/u on  $^{12}\text{C}$  and  $^{16}\text{O}$  at KVI, Groningen [26,27]. However, the  $(^3\text{He}, t)$  reaction at  $\sim 30$  MeV/nucleon was not suitable to strongly excite the spin-isospin resonances, because of a large contribution from the  $(^3\text{He}, d)(d, t)$  and  $(^3\text{He}, \alpha)(\alpha, t)$  sequential processes, which complicate the excitation mechanism and give non-negligible effects on the correlation patterns due to different substate populations. On the contrary, the  $(^3\text{He}, t)$  reaction at 450 MeV, or at higher bombarding energies, preferentially excites spin-isospin-flip modes [28]. This allows us to study the microscopic structure of charge-exchange spin-isospin modes [29–31]. In addition, a series of measurements of proton decays have been achieved at RCNP by means of the  $(^3\text{He}, t)$  reaction at 450 MeV [32–34]. In these previous works, proton angular correlations were, however, not so precisely measured, because of an insufficient angular correlation data of decay protons. The present experiments have been performed to obtain more precise angular correlations by using a silicon detector-array system. Therefore, in this paper, the angular correlations of proton decay induced by the  $^{12}\text{C}(^3\text{He}, t)$  reaction will be also reported and discussed.

## II. EXPERIMENT

The  $^{12}\text{C}(d, ^2\text{He} + n)$  and  $(^3\text{He}, t + p)$  reactions were measured using a deuteron beam at 200 MeV and a  $^3\text{He}$  beam at 450 MeV from the  $K=400$  MeV ring cyclotron at the Research Center for Nuclear Physics (RCNP), Osaka University.  $^3\text{He}$  and deuteron beams extracted from the ECR (Electron Cyclotron Resonance) ion source were accelerated by the  $K=120$  MeV AVF (Azimuthally Varying Field) cyclotron, and were further boosted to higher energies by the  $K=400$  MeV ring cyclotron. The extracted beam was achromatically transported from the ring cyclotron to the scattering chamber without any energy-defining slits in order to avoid a beam halo.

The beam-spot size was  $1 \text{ mm} \times 1 \text{ mm}$  in the vertical and horizontal directions. We used natural carbon targets for this experiment. The thicknesses of the targets were  $30 \text{ mg/cm}^2$  and  $2.0 \text{ mg/cm}^2$ , respectively for the  $(d, ^2\text{He} + n)$  and  $(^3\text{He}, t + p)$  experiments. The maximum beam currents on the target were 0.05 nA in the  $(d, ^2\text{He} + n)$  experiment and 3 nA in the  $(^3\text{He}, t + p)$  experiment. These rather weak beam currents were required to keep a good signal-to-noise ratio for the coincidence measurements of decay particles.

The time interval of the beam bunch was determined by the radio frequency of the AVF cyclotron. The deuteron and  $^3\text{He}$  beam frequencies of the AVF cyclotron were, respectively, 10.116 and 11.977 MHz, corresponding to the deuteron and  $^3\text{He}$  beam-repetition cycles of 98.85 ns and 83.49

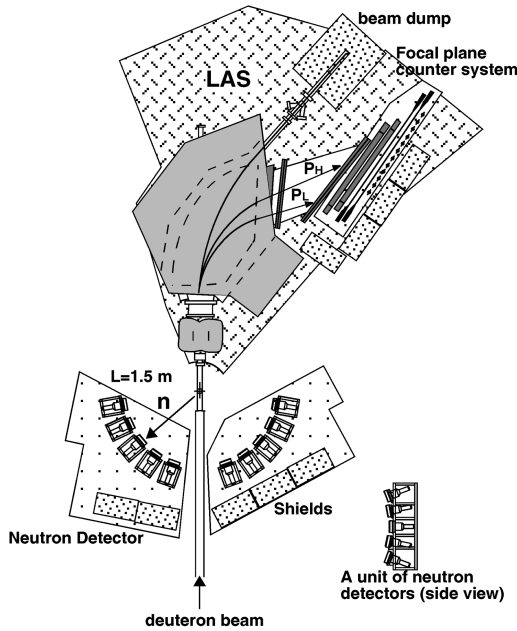


FIG. 2. Setup of the neutron scintillation-counter array for the measurement of neutron decay in coincidence with the  $(d, {}^2\text{He})$  reaction at zero degrees (top view). A side view of one set of the neutron detector array consisting of five liquid-scintillation counters is shown in the lower-right part of the figure. The  ${}^2\text{He}$  particles are identified as the two-proton unbound state. Two protons are measured in coincidence using the focal-plane counter system consisting of the trigger scintillator array and the multiwire drift counters. The trajectory information on two protons, e.g., indicated as  $P_H$  and  $P_L$  in the figure, are used to make the two-proton energy correlation for identification of a  ${}^2\text{He}$  particle. The incident deuteron beam is guided to the Faraday cup shielded with concrete blocks.

ns, respectively. In the neutron-decay measurement via the  $(d, {}^2\text{He})$  reaction, a beam buncher in the beam-transport system between the AVF and ring cyclotrons was used to avoid overlapping of neutron events and the pulsing ratio was chosen to be three, making a beam period of 296.6 ns.

### A. ${}^{12}\text{C}(d, {}^2\text{He}){}^{12}\text{B}$ Reaction

The outgoing  ${}^2\text{He}$  particles were measured by the coincidence detection procedure at zero degrees using the large-acceptance spectrometer (LAS) and its focal-plane counter system [35]. Figure 2 shows the experimental setup for the  $(d, {}^2\text{He}+n)$  measurement. The beam passing through the target was guided to an external beam dump through a beam extraction port of LAS. Two protons were bent in the LAS magnet and were measured in coincidence (denoted as  $P_H$  and  $P_L$  in Fig. 2, for example). Two protons with higher and lower energies were measured by the trigger scintillation-counter system consisting of six horizontal and 12 vertical plastic-scintillation counters. Light outputs from each horizontal-type scintillation counter were detected by two photomultipliers at both ends, while those from each vertical-type scintillation counter were detected by one photomultiplier.

Signals from the photomultiplier were divided by a divider circuit. The divided signals were sent to a constant-fraction discriminator (CFD) and to a charge-to-digital con-

verter (QDC). The QDC data were used for event discrimination of  $\gamma$  rays and protons. The translated logical signals by the CFD outputs from a horizontal scintillation counter were averaged in time using mean-timer modules. In order to identify two protons as a  ${}^2\text{He}$  event with a  ${}^1S_0$  ( $T=1$ ) configuration, trigger signals were generated from the coincidence events consisting of four signals from two horizontal plastic-scintillation counters and two vertical ones. The arrival positions of the two protons at the focal plane were determined with an accuracy of 0.3 mm using the multiwire drift chambers.

For the coincidence measurement of neutron decays following the  $(d, {}^2\text{He})$  reaction, we recently constructed a neutron multidetector array system, which is similar to the neutron-detector-array EDEN [36]. The neutron-detector array consisted of 48 identical BC-501A liquid-organic-scintillator cells with a diameter of 20 cm and a thickness of 5 cm. The liquid-organic scintillator BC-501A was deoxygenated and encapsulated in the air-tight aluminum cells for good pulse-shape discrimination. The inside of the cell was coated with MgO. The cell of the liquid scintillator had an optical window connected to a 5'' photomultiplier. Since neutron energies were measured by the time-of-flight (TOF) method with a short flight path of  $\sim 1.5$  m, the fast response property of the scintillator BC-501A was greatly helpful for the  $(d, {}^2\text{He}+n)$  experiment.

A set of five neutron detectors was mounted in the same steel frame with an aluminum spacer to incline each detector toward the target as shown at the lower-right part in Fig. 2. Ten units were installed on the steel stands. The center position of each unit was aligned at the same horizontal level of the beam line. Concrete shields were placed near the beam line and were used to decrease the level of neutron and  $\gamma$ -ray background. In order to measure the angular-correlation function of emitted neutrons, the detectors were positioned at backward angles from  $100^\circ$  to  $160^\circ$  in the laboratory system, because the neutron background from the deuteron-breakup reaction is small at backward angles. The detectors were classified into ten groups on the basis of angular position. The neutron flight distance between the target and the center of each neutron detector was  $1.50 \pm 0.02$  m. This detector geometry was chosen by considering the required energy resolution of neutrons and the geometrical restriction in setting the neutron detectors. The total solid angle was about 5% of  $4\pi$ .

The energy deposit of electrons is known to be proportional to the light-output of BC-501A in the range more than several tens keV electron-equivalent energy. The threshold voltage of the CFD was, thus, calibrated by measuring the  $\gamma$ -ray response of neutron detectors. The maximum energy of Compton-scattered electrons was determined by their edge in the fast-gated QDC spectrum.

The TOF of a neutron is given by  $T_n = (c_2 - c_1)t + t_\gamma$ , where  $c_1$  is the channel of the  $\gamma$ -flash peak position, which has been obtained during the run using an aluminum target of a thickness of 2 mm,  $c_2$  is the channel of the TDC obtained for the neutron events, and  $t_\gamma$  is the flight time of the  $\gamma$ -ray from the target to the detector. The accuracy of the time scale for  $t$  is determined by using the time calibrator.

The neutron decay energy from the 4.5 MeV state in  ${}^{12}\text{B}$  to the  $\frac{3}{2}^-$  ground state of  ${}^{11}\text{B}$  is 1.0 MeV (see Fig. 1). In

order to measure low-energy neutrons from the 4.5 MeV state, the threshold value of all the scintillation counters was set to  $\sim 40$  keV. Since the applied voltage to each photomultiplier was electronically limited to 3000 V, the CFD threshold voltages were set to be as low as possible. The neutron detection efficiency was estimated to be  $\sim 30\%$  with the threshold energy of 40 keV [37]. The energy resolution for the final-state spectrum was 600 keV.

### B. $^{12}\text{C}(^3\text{He},t)^{12}\text{N}$ reaction

The scattered tritons were analyzed by the spectrometer ‘‘GRAND RAIDEN’’ [38]. The experimental procedure and data-taking system were similar to those described previously [34]. The  $^3\text{He}^+$  particles, which were generated by the atomic charge-exchange process  $^3\text{He}^{++} \rightarrow ^3\text{He}^+$  in the target foil [39], were detected at the high momentum side of the focal-plane detector system and were used to check the beam resolution.

In the scattering chamber, forty Si(Li) solid-state detectors (SSD) were installed for measuring decay protons at backward angles. Each SSD was 5 mm in thickness and 400 mm<sup>2</sup> in effective area. Because of the thick SSD, we observe proton decays from the states in  $^{12}\text{N}$  with excitation energies up to  $E_x \sim 30$  MeV. The total solid angle covered by the SSD’s was 3% of  $4\pi$ . The SSD’s were located at backward angles with respect to the incident  $^3\text{He}$  beam to avoid detection of the background protons due to the quasielastic charge-exchange knockon process and the  $^3\text{He} \rightarrow p + d$  breakup reactions at forward angles.

The SSD’s were assembled on 2 mm thick plates connected to a cooling pipe through which coolant liquid with temperature of a  $-20$  °C was circulated. The thermal noise of each SSD was greatly reduced by cooling, and the energy resolution was improved. Using the  $^{241}\text{Am}$   $\alpha$  source, the energy resolution of each detector was checked to be less than 50 keV in the off-line test. The final-state energy resolution in the actual experiment was, however, in the range of 350–450 keV. This was due to (1) the increase of noise levels due to the irradiation of SSD’s by electrons and  $\gamma$  rays, (2) the energy loss of decay protons in the target, and (3) the beam energy resolution. The difference of the energy losses of  $^3\text{He}$  and tritons in the 2 mg/cm<sup>2</sup> carbon target was relatively small.

## III. DATA REDUCTION AND RESULTS

### A. Data analysis of the $^{12}\text{C}(d,^2\text{He})^{12}\text{B}$ reaction

The maximum effective solid angle was estimated to be 2.4 msr for the  $(d,^2\text{He})$  measurement with the LAS for the maximum accepted relative energy  $\varepsilon_{\text{max}} = 5$  MeV [40]. The energy calibration of the  $(d,^2\text{He})$  spectra was made by using various sharp peaks for the states in  $^{10}\text{Be}$ ,  $^{11}\text{Be}$ , and  $^{12}\text{B}$ . Figure 3 displays the  $^{10,11}\text{B}(d,^2\text{He})^{10,11}\text{Be}$  spectra taken at  $E_d = 200$  MeV. We observe several sharp peaks at 3.37, 5.96, and 9.3 MeV in  $^{10}\text{Be}$  and at 0.3, 2.7, and 3.9 MeV in  $^{11}\text{Be}$ . These correspond to the Gamow-Teller transitions to states in  $^{10}\text{Be}$  and  $^{11}\text{Be}$ . The resolution achieved for these two reactions was 400 keV, essentially determined by the beam and spectrometer resolutions. In addition, we observe a broad bump corresponding to the transition to the spin-dipole

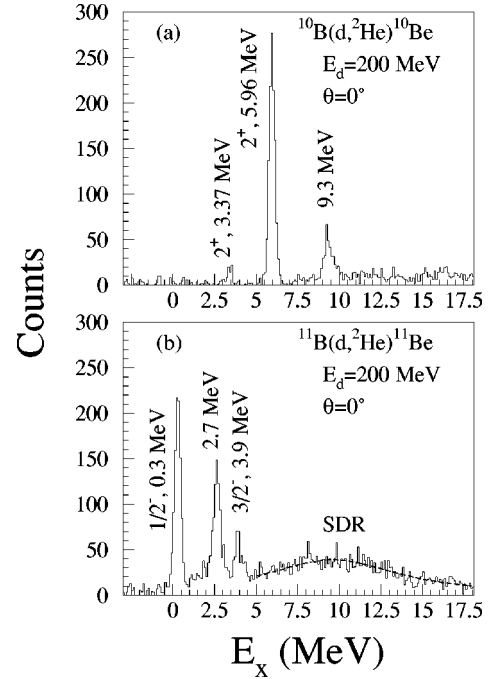


FIG. 3. Excitation-energy spectra at  $\theta = 0^\circ$  for (a) the  $^{10}\text{B}(d,^2\text{He})^{10}\text{Be}$  and for (b) the  $^{11}\text{B}(d,^2\text{He})^{11}\text{Be}$  reactions measured at  $E_d = 200$  MeV. The thicknesses of the  $^{10}\text{B}$  and  $^{11}\text{B}$  targets were 15.8 and 15.0 mg/cm<sup>2</sup>, respectively. Accidental coincidence events have been subtracted. Sharp peaks denoted by their excitation energies and  $J^\pi$  values are due to the Gamow-Teller transitions. A broad bump corresponding to the spin-flip dipole resonance in  $^{11}\text{Be}$  is observed in the  $^{11}\text{B}(d,^2\text{He})^{11}\text{Be}$  reaction.

resonance (SDR) in  $^{11}\text{Be}$ . Using various discrete peaks in the  $(d,^2\text{He})$  reactions on  $^{10,11}\text{B}$  and  $^{12}\text{C}$ , we could reliably confirm a good linear relation of the excitation energy versus the focal-plane position.

The underlying background in the  $^{10,11}\text{B}(d,^2\text{He})^{10,11}\text{Be}$  spectra (see Fig. 3) was mainly due to events induced by neutrons associated with the deuteron-breakup reaction. After cutting out the part of the two-dimensional spectrum due to the random coincidences of neutrons with the very strong  $(d,^2\text{He})$  transition to the  $1^+$  ground state of  $^{12}\text{B}$ , the prompt-to-random ratio of the time peaks improved to 2.9 from 1.1. To obtain the true-coincidence final-state spectra and  $^2\text{He}$  coincidence spectra, random spectra were subtracted from the prompt ones.

### B. Data analysis of the $^{12}\text{C}(^3\text{He},t)^{12}\text{N}$ reaction

Energy calibration was performed using the  $^{12}\text{C}(^3\text{He},t)^{12}\text{N}$  reaction. Since the ratio of the isotopic abundance for  $^{12}\text{C}$  and  $^{13}\text{C}$  is 98.89%:1.11%, we observe several peaks corresponding to the discrete states excited by the  $^{12}\text{C}(^3\text{He},t)^{12}\text{N}$  and  $^{13}\text{C}(^3\text{He},t)^{13}\text{N}$  reactions. The  $^{12}\text{C}(^3\text{He},t)^{12}\text{N}$  reaction has a large negative- $Q$  value of  $-17.355$  MeV. On the other hand, the  $^{13}\text{C}(^3\text{He},t)^{13}\text{N}$  reaction has a comparatively small- $Q$  value of  $-2.239$  MeV. It was, therefore, possible to calibrate the  $(^3\text{He},t)$  energy spectrum using the well-known discrete states in  $^{13}\text{N}$  and  $^{12}\text{N}$ . The variation in the beam energy during the experiment was corrected for by using the  $^3\text{He}^+$  peak, produced by the atomic charge-exchange reaction [39] of the incident  $^3\text{He}^{++}$ , as a calibration monitor.

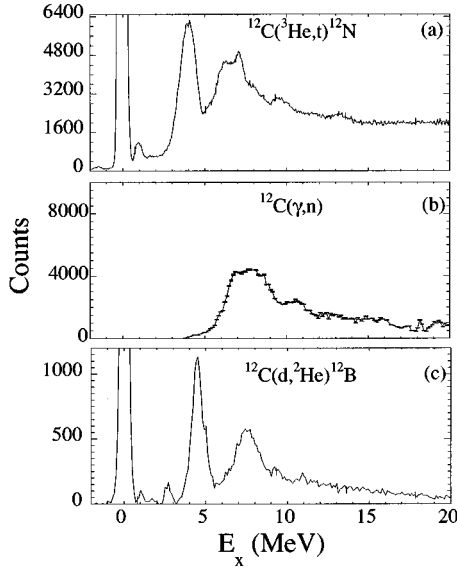


FIG. 4. The excitation-energy spectra of  $^{12}\text{N}$  and  $^{12}\text{B}$  from the charge-exchange reactions (a)  $^{12}\text{C}(^3\text{He},t)$ , and (b)  $^{12}\text{C}(d,^2\text{He})$ , respectively, in comparison with (c) the  $^{12}\text{C}(\gamma,n)$  spectrum taken from Ref. [9] and shifted by 15.1 MeV.

In the present experiments, the ratio of the true-to-random coincidences was 6:1, which was estimated from the coincidence-timing spectrum. The random events were subtracted from the prompt events in all the coincidence spectra.

### C. Singles spectra

Figure 4 compares the three spectra obtained from the ( $^3\text{He},t$ ), ( $\gamma,n$ ), and ( $d,^2\text{He}$ ) reactions on  $^{12}\text{C}$ . The singles spectrum for the  $^{12}\text{C}(^3\text{He},t)^{12}\text{N}$  reaction at  $E(^3\text{He})=450$  MeV at zero degrees is shown in Fig. 4(a). The energy resolution of the ( $^3\text{He},t$ ) measurement for the  $1^+$  ground state of  $^{12}\text{N}$  was 320 keV. Fujiwara *et al.* reported [28] that the ratio of the excitation strengths between the ground state of  $^{12}\text{N}$  and the state at  $E_x=3.51$  MeV of  $^{13}\text{N}$  closely agrees with the results of charge-exchange ( $^3\text{He},t$ ) reactions at higher energies [41]. Thus, the reaction mechanism of the ( $^3\text{He},t$ ) reaction at  $E(^3\text{He})=450$  MeV is considered to be similar to that of the ( $p,n$ ) reaction at high incident energies where the eikonal approximation is applicable.

The strongest peak at  $E_x=0$  MeV is the dominant  $\Delta L=0$  transition to the  $1^+$  ground state of  $^{12}\text{N}$ . A small peak at  $E_x=0.96$  MeV corresponds to the  $2^+$  first-excited state. There are two broad peaks located at  $E_x\approx 4.1$  and 7 MeV in the  $^{12}\text{C}(^3\text{He},t)^{12}\text{N}$  spectrum. The first broad peak at  $E_x\approx 4.1$  MeV, and the second broad peak at  $E_x\approx 7$  MeV correspond to the spin-dipole transitions. The spin and parity of the broad peak at 4.1 MeV has been assigned to be  $2^-$ . The full width at half maximum (FWHM) is 1.4 MeV. Although  $^{12}\text{N}$  and  $^{12}\text{B}$  are mirror nuclei, the energy and width for analog resonances in the spectra of  $^{12}\text{N}$  and  $^{12}\text{B}$  differ significantly from each other.

The second large broad peak at 7 MeV has a width of 4.0 MeV. The ( $1^-$ ) peak structures around 7 MeV are different in  $^{12}\text{N}$  and  $^{12}\text{B}$ . In the  $^{12}\text{C}(^3\text{He},t)^{12}\text{N}$  spectrum, the broad peak at  $\sim 7$  MeV seems to consist of several sharp peaks. At least, there are two peaks at 6.4 MeV and 7.1 MeV. Since the

magnitude of the spin-flip term  $V_{\sigma\tau}$  of the effective interaction is much larger than the non-spin-flip term  $V_\tau$  in the incident energy region of 100~150 MeV/nucleon [42,43], the non-spin-flip excitation is considered to be still small. However, appreciable contributions from the non-spin-flip strengths can be expected in the  $^{12}\text{C}(^3\text{He},t)^{12}\text{N}$  spectrum if the transition amplitude to a final state were large. Sterrenburg *et al.* [26] reported that a sharp state with a low spin is observed at  $E_x=7.63$  MeV in the  $^{12}\text{C}(^3\text{He},t)^{12}\text{N}$  reaction at  $E(^3\text{He})=81$  and 75 MeV, and that this state strongly decays by proton emission into the  $\frac{5}{2}^-$  state in  $^{11}\text{C}$ . The 7.63 MeV state reported in Ref. [26] is, however, not strongly seen in the present singles ( $^3\text{He},t$ ) measurement. On the other hand, we observed a sharp peak at 7.1 MeV, which might correspond to the  $7.40\pm 0.05$  MeV ( $1^-$ ) state reported in Ref. [14].

There is a broad peak at  $E_x\approx 10$  MeV, which is also observed in the ( $p,n$ ) reaction [15]. There is a small bump at  $E_x\approx 13$  MeV, but this bump on top of the continuum region due to the quasifree process is not observed in other charge-exchange reactions.

Figure 4(c) shows a spectrum for the  $^{12}\text{C}(d,^2\text{He})^{12}\text{B}$  reaction at  $\theta\approx 0^\circ$ . The backgrounds, which were due to the  $p+n$  breakup yields and due to the random coincidence events from two protons triggering in neighboring beam bursts, were subtracted in making the final singles spectrum in Fig. 4(c). The spectrum for the  $^{12}\text{C}(d,^2\text{He})^{12}\text{B}$  reaction at 200 MeV is remarkably similar to that at  $E_d=260$  MeV [20]. This indicates that the ( $d,^2\text{He}$ ) reaction mechanism at  $E_d=200$  MeV is simple as that at  $E_d=260$  MeV and that the observed states are excited with pure spin-flip ( $\Delta S=1$ ) transitions.

The narrow peak of the ground state of  $^{12}\text{B}$  corresponds to the  $1^+$  Gamow-Teller state which is governed by the transition with a simple  $1p_{3/2}\rightarrow 1p_{1/2}$  matrix element. The energy resolution of the ( $d,^2\text{He}$ ) measurement was 380 keV for the peak of the  $1^+$  ground state of  $^{12}\text{B}$ . Three small peaks in the region of  $E_x=0.9-3$  MeV correspond to the  $2^+$ ,  $2^-$ , and  $1^-$  states at  $E_x=0.95$ , 1.67, and 2.62 MeV, respectively [14]. There are two broad peaks located at  $E_x=4.5$  and 7.7 MeV in the spectrum [see Fig. 4(c)].

The broad peak at 4.5 MeV is well known to be the spin-flip dipole resonance with  $J^\pi=2^-$ . The full width at half maximum (FWHM) of this broad peak was 0.8 MeV including the beam resolution. If the observed width ( $\Gamma_{\text{obs}}$ ), the intrinsic width ( $\Gamma_{\text{int}}$ ), and the experimental width ( $\Gamma_{\text{res}}$ ) are assumed to have a relation as  $\Gamma_{\text{obs}}^2 = \Gamma_{\text{int}}^2 + \Gamma_{\text{res}}^2$ , we get  $\Gamma_{\text{int}} = 0.69$  MeV for the  $2^-$  state in  $^{12}\text{B}$  and  $\Gamma_{\text{int}} = 1.36$  MeV for the  $2^-$  state in  $^{12}\text{N}$ . The width  $\Gamma_{\text{int}}=1.36$  MeV for the  $2^-$  state in  $^{12}\text{N}$  is much wider than the value of  $0.83\pm 0.02$  MeV given in Ref. [14]. On the other hand, the width of 0.69 MeV for the  $2^-$  resonance at 4.5 MeV in  $^{12}\text{B}$  is much narrower. Thus, one should conclude that the broad peak at 4.1 MeV observed in the  $^{12}\text{C}(^3\text{He},t)^{12}\text{N}$  reaction at 450 MeV consists of several unresolved peaks. Presumably, a non-spin-flip state exists on the lower excitation-energy shoulder of the 4.1 MeV broad peak in the  $^{12}\text{C}(^3\text{He},t)^{12}\text{N}$  spectrum. This shoulder peak may correspond to the 3.53 MeV ( $1^-$  or  $2^+$ ) state reported in Ref. [14]. Since the excitation of a  $2^+$  state is expected to be relatively weak in the high-energy ( $^3\text{He},t$ )

reaction, the spin and parity assignment of the 3.53 MeV state is favored to be  $1^-$ .

The second broad peak at 7.7 MeV in  $^{12}\text{B}$  has a width of 4.0 MeV. In contrast to the  $^{12}\text{C}(^3\text{He},t)^{12}\text{N}$  spectrum in Fig. 4(a), the sharp peaks at around 7 MeV are not observed in the  $^{12}\text{C}(d,^2\text{He})^{12}\text{B}$  reaction although several broad and sharp  $1^-$  states at 6.0 MeV, 7.06 MeV,  $7.7 \pm 0.1$  MeV,  $7.836 \pm 0.02$  MeV, and  $7.937 \pm 0.02$  MeV are expected in  $^{12}\text{B}$  [14]. Obviously, the peak structure at  $E_x = 6.4$  and 7.1 MeV in the  $^{12}\text{C}(^3\text{He},t)^{12}\text{N}$  reaction does not appear in the  $^{12}\text{C}(d,^2\text{He})^{12}\text{B}$  spectrum [shown in Fig. 4(c)]. Therefore, the differences between the two mirror spectra of  $^{12}\text{N}$  and  $^{12}\text{B}$  excited by the  $(^3\text{He},t)$  and  $(d,^2\text{He})$  reactions, respectively, can be attributed to the fact that whereas  $(d,^2\text{He})$  reaction only excites spin-flip states, the  $(^3\text{He},t)$  reaction excites collective non-spin-flip states as well although weakly.

The  $^{12}\text{C}(\gamma,n)$  spectrum presented in Fig. 4(b) [9] is compared with the  $(^3\text{He},t)$  and  $(d,^2\text{He})$  spectra. The  $^{12}\text{C}(\gamma,n)$  reaction dominantly measures the non-spin-flip  $1^-$ ,  $T=1$  states in  $^{12}\text{C}$ . As far as the isobaric spin is a good quantum number, the giant  $E1$  resonance observed in the  $^{12}\text{C}(\gamma,n)$  reaction should have analog  $1^-$  excitations in both the  $(^3\text{He},t)$  and  $(d,^2\text{He})$  reactions. Because of this, the excitation energy of the  $^{12}\text{C}(\gamma,n)$  spectrum [9] is shifted by 15.1 MeV to compare the  $T=1$  analog states in the isospin-triplet nuclei. We observe the broad bump of the  $E1$  resonance, which corresponds to the resonance situated at  $\sim 7$  MeV in  $^{12}\text{B}$  and  $^{12}\text{N}$ , although the  $E1$  GDR should not be excited in  $^{12}\text{B}$  in the  $(d,^2\text{He})$  reaction. The resonance in  $^{12}\text{N}$  observed in the  $(^3\text{He},t)$  reactions is expected to carry a large  $1^-$  strength including both the spin-flip and non-spin-flip components. In the angular distribution analysis of the  $^{12}\text{C}(p,n)$  reaction [15], the spin and parity assignment for the 7 MeV peak is consistent with the assumption that there exists a strongly excited  $1^-$  state at  $E_x \sim 7$  MeV, where theoretical calculations predict the presence of both spin-flip and non-spin-flip  $1^-$  states [44–46]. The broad bump at 7 MeV was also observed in the non-spin-flip spectrum from the  $^{12}\text{C}(^7\text{Li},^7\text{Be})$  reaction [25].

There is a peak at  $E_x \sim 10.0$  MeV in the  $^{12}\text{C}(^3\text{He},t)^{12}\text{N}$  spectrum. This is the analog of a broad peak observed at  $E_\gamma = 25.5$  MeV in the  $^{12}\text{C}(\gamma,n)$  spectrum [9]. The  $^{12}\text{C}(d,^2\text{He})^{12}\text{B}$  reaction should not excite the analog of the broad peak observed in the  $^{12}\text{C}(\gamma,n)$  reaction because it selectively excites spin-flip states only. A very small bump is observed at  $\sim 10.0$  MeV in the  $^{12}\text{C}(d,^2\text{He})^{12}\text{B}$  reaction.

#### D. Coincidence spectra

##### 1. Neutron decay from $^{12}\text{B}$

A two-dimensional scatter plot is shown in Fig. 5(a) for neutron decays from the excited states in  $^{12}\text{B}$ . Triple-coincidence events for two protons at  $\theta=0^\circ$  identified as the  $^1S_0$ ,  $^2\text{He}$  state and a decay neutron are represented by dots in the two-dimensional plane of the neutron decay energy versus the excitation energy in  $^{12}\text{B}$ . The decay loci to the final states in  $^{11}\text{B}$  are recognized in Fig. 5(a) although random coincidence events are not negligible. The ratio of the true-to-random coincidence events gated on the ground state of  $^{11}\text{B}$  was quite good (see Fig. 5), despite the difficult

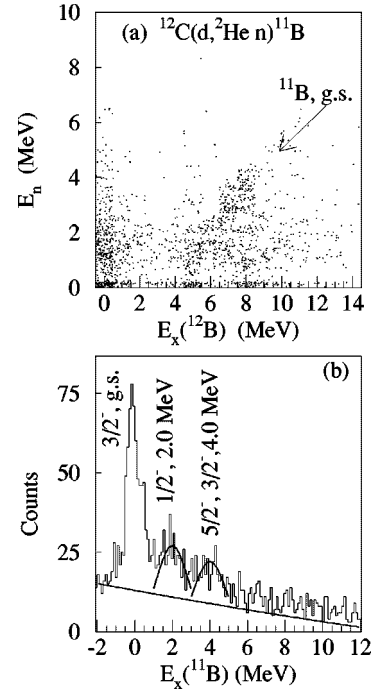


FIG. 5. (a) The two-dimensional coincidence spectrum of the  $^{12}\text{C}(d,^2\text{He}+n)$  reaction, and (b) a projected spectrum of neutron decays from the intermediate excited states in  $^{12}\text{B}$  to the final states in  $^{11}\text{B}$ .

neutron-coincidence experiment. This did not depend much on the neutron detector or its angle in the angular range measured, i.e.,  $100^\circ$ – $160^\circ$ .

The total counts of decay neutrons from the 4.5 MeV bump in  $^{12}\text{B}$  to the ground state of  $^{11}\text{B}$  was smaller than the decay neutron events from the 7.7 MeV bump. Since the neutron separation energy ( $S_n=3.7$  MeV) is close to the SDR at 4.5 MeV, the available neutron energy is small. Because of this, the penetrabilities of neutrons from  $^{12}\text{B}$  are small and were calculated to be 0.2 for  $l=2$  decay to the ground state of  $^{11}\text{B}$  at the excitation energy of 4.5 MeV in  $^{12}\text{B}$ . The wave function of the  $2^-$ , SDR at 4.5 MeV is expected to have a main  $(\pi p_{3/2}^{-1} \nu d_{5/2})$  configuration. Thus, the direct neutron decay occurs largely with  $l=2$ , and is rather hindered. In addition, the electronic threshold artificially contributes to lowering the number of detected events from the 4.5 MeV bump to the ground state of  $^{11}\text{B}$ . Therefore, the observed neutron decay from the SDR at  $E_x(^{12}\text{B})=4.5$  MeV is small.

The loci for neutron decay of the SDR at  $E_x=4.5$  and 7.7 MeV to the ground state and the low-lying proton-hole states in  $^{11}\text{B}$  were observed [shown in Fig. 5(a)]. Figure 5(b) shows a spectrum of neutron decays projected onto the excitation-energy axis of  $^{11}\text{B}$ . The peak of neutron decay into the  $\frac{3}{2}^-$  ground state of  $^{11}\text{B}$  is prominent. This is due to the strong neutron decay from the 7.7 MeV bump, which is seen in the two-dimensional scatter plot of Fig. 5(a). Neutron decay to the  $\frac{1}{2}^-$ ,  $\frac{5}{2}^-$ , and  $\frac{3}{2}^-$  states in  $^{11}\text{B}$  is also observed although the resolution for neutron detection is not sufficient to separate the final states. The angular correlation for neutron decay from the  $E_x(^{12}\text{B})=7.7$  MeV bump region to the ground state of  $^{11}\text{B}$  was determined. Figure 6 displays the results.

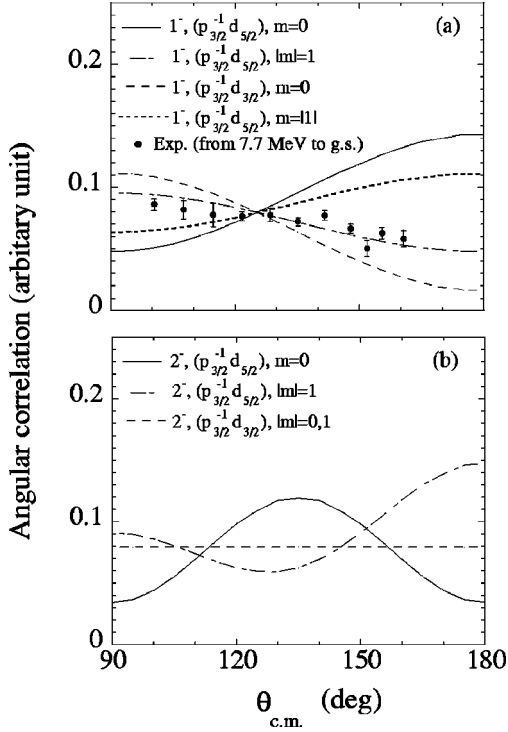


FIG. 6. Angular correlation of decay neutrons from the SDR region at 7.7 MeV in  $^{12}\text{B}$  to the ground state of  $^{11}\text{B}$ . The angular-correlation patterns calculated for neutron decay from the  $2^-$  and  $1^-$  states to the ground state of  $^{11}\text{B}$  are compared with the experimental data. It is assumed that the  $2^-$  and  $1^-$  states have  $(p_{3/2}^{-1}d_{3/2})$  and  $(p_{3/2}^{-1}d_{3/2})$  configurations, and are excited with the substate populations of  $|m|=0,1$ . (a) The solid, dash-dotted, dashed, and dotted lines are the results of calculations with the ANGCOR code for a  $1^-$  excitation with the assumptions indicated in the figure. (b) The same as in (a), but for a  $2^-$  excitation. The angular correlations from the  $2^-$  states with  $(p_{3/2}^{-1}d_{3/2})$  configurations are isotropic.

## 2. Proton decay from $^{12}\text{N}$

Two-dimensional scatter plots of proton energies measured versus the excitation energies in  $^{12}\text{N}$  were generated by subtracting random events from prompt events in a similar procedure to that described in Ref. [34]. The separation energy ( $S_p$ ) for proton decay is 0.6 MeV in  $^{12}\text{N}$ . On the other hand, the neutron separation energy ( $S_n$ ) is 15.7 MeV (see Fig. 1). Thus, proton decay is the main decay channel for the excitation energy region  $E_x=0.6-15.7$  MeV. Figure 7(a) shows a prompt two-dimensional spectrum, which is obtained by gating on the solid angle centered at zero degrees. Loci associated with decay from the SDR and higher-lying excitations to the ground state and the low-lying neutron-hole states in  $^{11}\text{C}$  can be clearly seen. The final-state spectrum obtained by projecting the two-dimensional scatter plot is shown in Fig. 7(b). The final states in  $^{11}\text{C}$  are evident for the  $\frac{3}{2}^-$  g.s.,  $\frac{1}{2}^-$ ,  $\frac{5}{2}^-$ ,  $\frac{3}{2}^-$ , and  $\frac{1}{2}^+$  states, which have been observed in the  $(^3\text{He},t+p)$  work by Sterrenburg *et al.* [26]. In addition, we clearly identify the proton decay to the  $\frac{1}{2}^-$ , 8.1 MeV state in  $^{11}\text{C}$ .

It is worth noting that proton decays from the highly excited continuum states in  $^{12}\text{N}$  to the ground state in  $^{11}\text{C}$  are observed without any sudden decrease even when the neutron-decay channel opens. This fact suggests that since the present  $(^3\text{He},t)$  reaction at 450 MeV excites the states

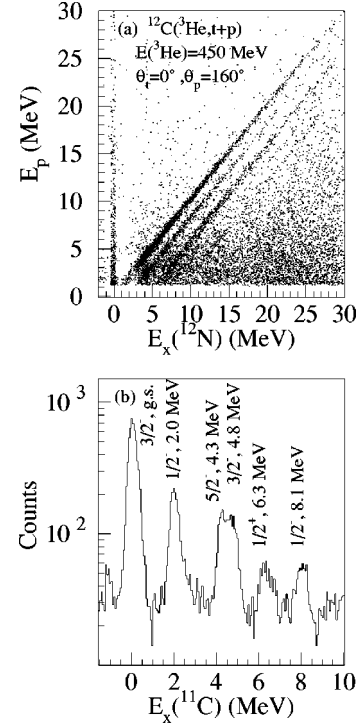


FIG. 7. (a) Two-dimensional scatter plot of proton-triton coincidence events induced by the  $^{12}\text{C}(^3\text{He},t)$  reaction at  $\theta=0^\circ$ . The loci indicate proton decay to final states in  $^{11}\text{C}$ . Proton events with energies lower than  $\sim 1.2$  MeV are cut off by an electronic threshold. (b) The final-state spectrum of  $^{11}\text{C}$  obtained by projecting loci in the scatter plot onto the excitation energy axis of  $^{11}\text{C}$ .

with one-proton-particle one-neutron-hole ( $1p-1h$ ) configurations, neutron decay is strongly suppressed even when the neutron-decay channel opens.

Since the penetration thickness of protons in the carbon target depends on the emission angles of protons, the energy loss of decay protons in the carbon target with a thickness of  $2\text{ mg/cm}^2$  varies from 0 to 250 keV for protons with a decay energy of 1 MeV. Therefore, a good energy resolution is obtained for the SSD located at backward angles. The energy resolution of the final-state spectrum varied in the range 350–450 keV, depending on the emission angles. The obtained resolution was sufficient to resolve the decay events to the ground state and the first excited state at 2 MeV in contrast to the case of the neutron-decay measurements. However, it was not sufficient to resolve well the decay into two states at 4.3 and 4.8 MeV in  $^{11}\text{C}$ .

In order to get the angular correlations of proton decay, the bump structures and the continuum region of the  $^{12}\text{C}(^3\text{He},t)^{12}\text{N}$  spectrum were divided into different bins as indicated in Fig. 8. These are similar to regions that have been used earlier by Sterrenburg *et al.* [26] in the  $^{12}\text{C}(^3\text{He},t)$  reaction at 81 MeV, because they defined observed peaks corresponding to resonance structures. The angular correlations obtained in the present experiment are shown in Figs. 9–13 and their numerical values are listed in Tables I–III.

We took special care in obtaining the experimental data of the angular correlations, since the presented results were sensitive to the electronic threshold in detecting low-energy protons. In the present analyses, the proton events with  $E_{\text{decay}}(p) < 1.2$  MeV were excluded in the event accumula-

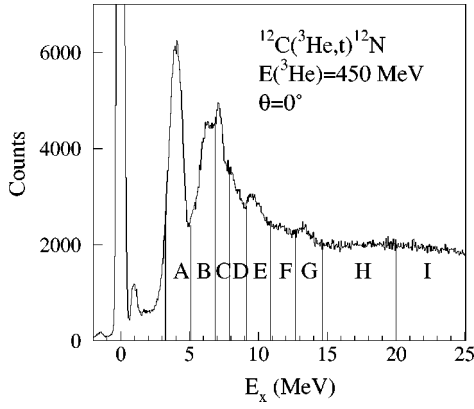


FIG. 8. A singles spectrum at  $\theta=0^\circ$  for the  $^{12}\text{C}(^3\text{He},t)^{12}\text{N}$  reaction at  $E(^3\text{He})=450$  MeV. The regions denoted as A–I indicate the gating bins for which angular-correlation patterns for proton decay into the final states in  $^{11}\text{C}$  have been determined.

tion. Therefore, the data for proton decay from region A to  $E_x(^{11}\text{C}) = 2.0$  MeV are not reliable, and are not shown in the present paper.

The correlation patterns observed for protons decaying to the ground state of  $^{11}\text{C}$  are found to be smooth and well fitted by the Legendre polynomials:

$$W(\theta) = A_0[1 + a_2P_2(\cos\theta) + a_4P_4(\cos\theta)]. \quad (1)$$

In general, the branching ratios from each excitation energy region for decay into various channels can depend on

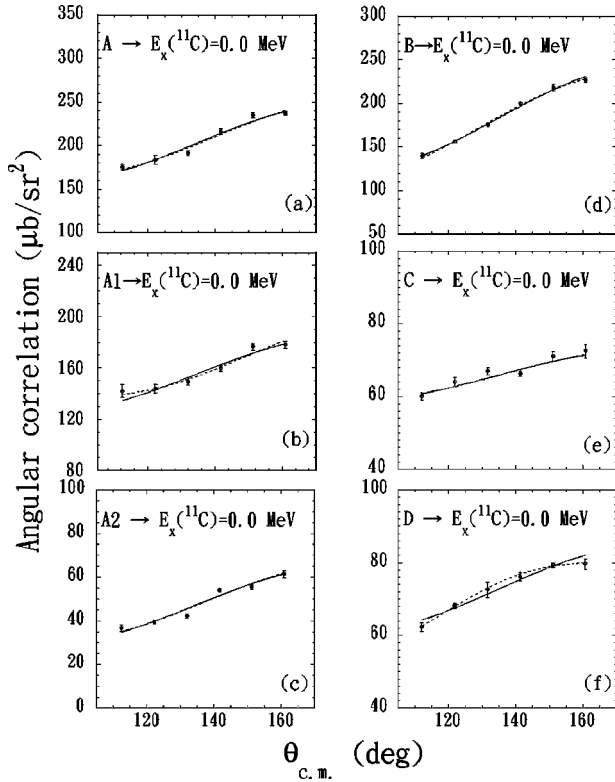


FIG. 9. The angular-correlation patterns of decay protons from the excited states in  $^{12}\text{N}$  (regions A–D) to the  $\frac{3}{2}^-$  ground state of  $^{11}\text{C}$ . The solid line shows the results of the fits with a constant plus Legendre function  $P_2(\cos\theta)$ . The dashed line is the fit including in addition a  $P_4(\cos\theta)$  term [see Eq. 1].

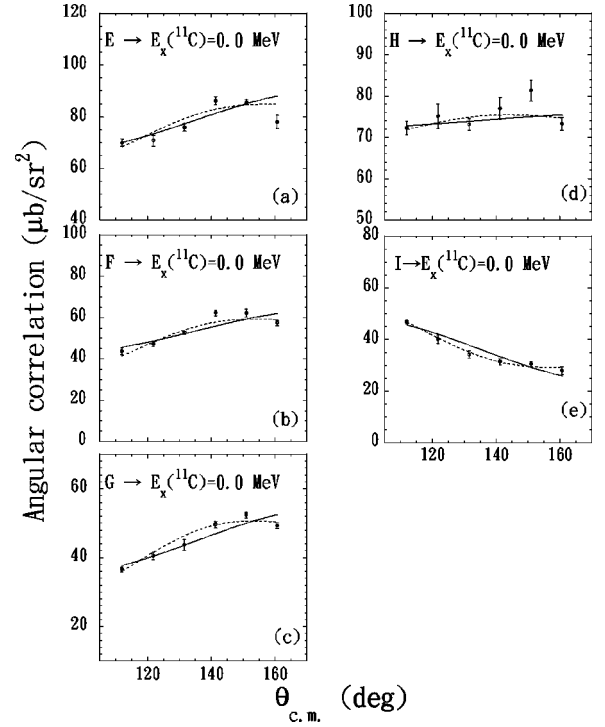


FIG. 10. Same as Fig. 9, but for regions E–I.

penetrabilities of the Coulomb and centrifugal barriers as well as the nuclear wave functions. In  $^{12}\text{N}$ , the Coulomb and centrifugal barriers for proton decay are small, implying a branching ratio of unity for proton decay. However, because of the high threshold effects of the SSD's, the measured branching ratio for proton decay seems effectively to be smaller than unity.

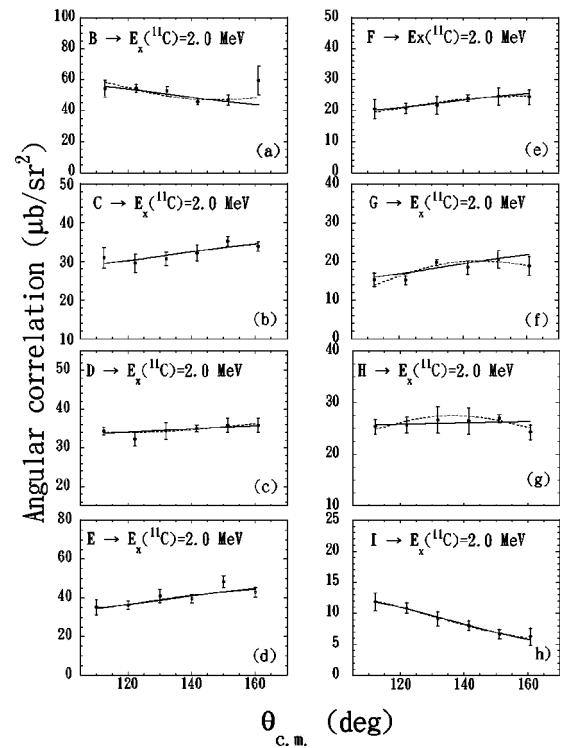


FIG. 11. Same as Fig. 9, but for decay from regions B–I to the  $2.0$  MeV  $\frac{1}{2}^-$  state in  $^{11}\text{C}$ .

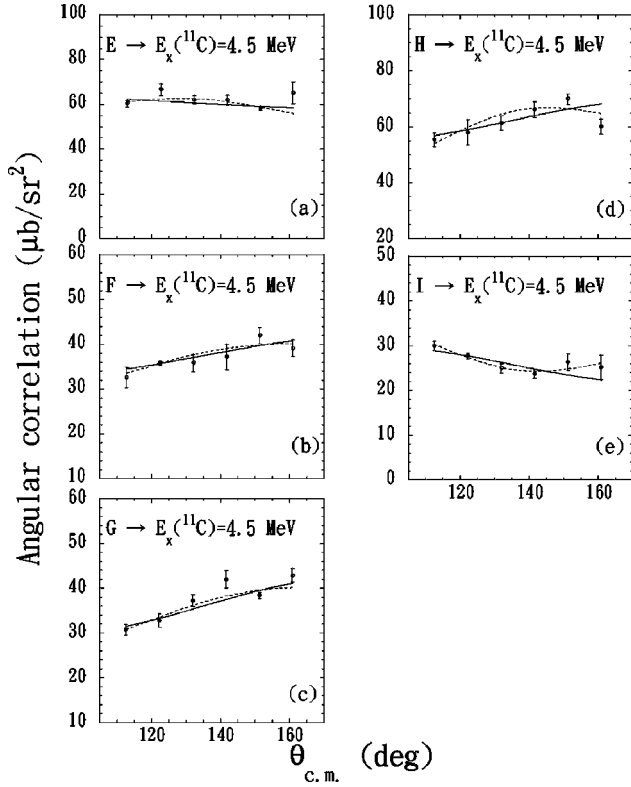


FIG. 12. Same as Fig. 9, but for decays from regions E–I to the two states at 4.3 and 4.8 MeV in  $^{11}\text{C}$ .

#### IV. DISCUSSION

##### A. Structure of $^{12}\text{B}$

In the recent reports of the  $^{12}\text{C}(\vec{d}, ^2\text{He})$  and  $^{12}\text{C}(^{12}\text{C}, ^{12}\text{N})$  experiments in RIKEN [18,48], it was concluded that the large bump at  $E_x(^{12}\text{B})=7.5$  MeV should be attributed to the dominant  $2^-$  excitation. If this conclusion were right, we have to address a new problem to solve the contradictory ( $p, n$ ) results at intermediate energies [15,16,49,50] and the theoretical calculations predicting a strong  $1^-$  state centered

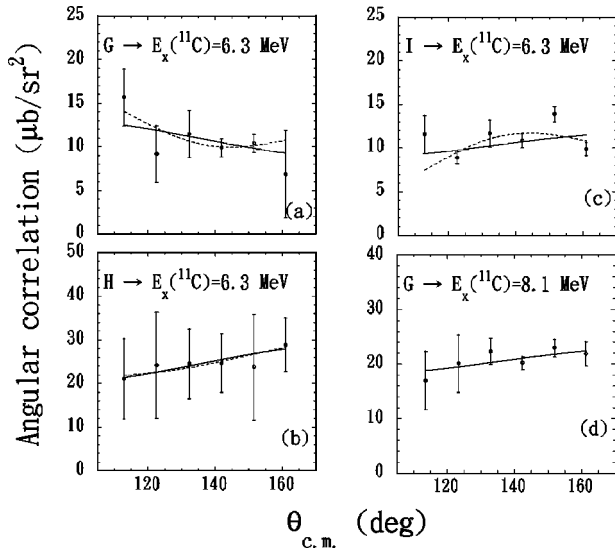


FIG. 13. Same as Fig. 9, but for decay from regions G–I to the higher excited states in  $^{11}\text{C}$ .

TABLE I. Coefficients of the Legendre polynomials fitted to the angular correlations of decay protons from the  $^{12}\text{N}$  excited states in the excitation-energy regions A–I to the ground state. The coefficients are derived from the fits of the first one or both terms of the Legendre polynomials in Eq. (1) (upper and lower parts in each column).

Region	Proton decay to the ground state of $^{11}\text{C}$		
	$A_0(\mu\text{b}/\text{sr}^2)$	$a_2$	$a_4$
A	$188.3 \pm 1.8$	$0.32 \pm 0.02$	
	$189.6 \pm 2.3$	$0.30 \pm 0.03$	$0.02 \pm 0.03$
A1	$145.7 \pm 1.9$	$0.27 \pm 0.03$	
	$149.4 \pm 2.8$	$0.22 \pm 0.04$	$0.06 \pm 0.04$
A2	$41.5 \pm 0.5$	$0.57 \pm 0.04$	
	$41.8 \pm 0.9$	$0.56 \pm 0.02$	$0.05 \pm 0.04$
B	$163.1 \pm 1.0$	$0.50 \pm 0.02$	
C	$161.1 \pm 1.6$	$0.52 \pm 0.03$	$-0.00 \pm 0.03$
	$63.5 \pm 0.5$	$0.15 \pm 0.02$	
D	$63.6 \pm 0.7$	$0.15 \pm 0.02$	$0.00 \pm 0.03$
	$68.8 \pm 0.5$	$0.23 \pm 0.01$	
E	$67.5 \pm 0.7$	$0.27 \pm 0.02$	$-0.00 \pm 0.03$
	$74.7 \pm 0.8$	$0.21 \pm 0.02$	
F	$73.1 \pm 1.0$	$0.25 \pm 0.03$	$-0.10 \pm 0.04$
	$49.8 \pm 0.6$	$0.29 \pm 0.03$	
G	$46.8 \pm 0.9$	$0.43 \pm 0.05$	$-0.10 \pm 0.05$
	$41.5 \pm 0.5$	$0.32 \pm 0.02$	
H	$40.4 \pm 0.5$	$0.41 \pm 0.31$	$-0.10 \pm 0.04$
	$73.5 \pm 0.9$	$0.03 \pm 0.02$	
I	$72.9 \pm 1.1$	$0.06 \pm 0.03$	$-0.00 \pm 0.04$
	$40.5 \pm 0.5$	$-0.43 \pm 0.03$	
	$41.5 \pm 0.6$	$-0.47 \pm 0.03$	$0.19 \pm 0.05$

at 7 MeV [44–46]. For example, a recent theoretical calculation by Anderson *et al.* [15] shows that there are three excited  $1^-$  states at  $E_x=7.1$ , 7.8, and 8.5 MeV with the  $(1p_{3/2}^{-1}1d_{5/2})$  and/or  $(1p_{3/2}^{-1}1d_{3/2})$  configurations, and that some  $2^-$  strength is predicted at 6.1 and 6.8 MeV with the  $(1p_{3/2}^{-1}1d_{3/2})$  configuration.

The present experiment indicates that the angular-correlation pattern for neutron decay from the 7.7 MeV large bump to the ground state of  $^{11}\text{B}$  is best fitted with the assumption that the wave function of the 7.7 MeV state mainly consists of a  $1^-$  state with the  $(1p_{3/2}^{-1}1d_{5/2})$  configuration. In the analyses of the angular correlation of neutron decay from the 7.7 MeV resonance, we put a simple assumption that the magnetic substates of the 7.7 MeV resonance are aligned to only  $m=0, \pm 1$ . This assumption is reasonable since we measure the ejected particles  $^2\text{He}$  at zero degrees. Then, we calculated the angular correlations from the  $1^-$  and  $2^-$  states with the  $(1p_{3/2}^{-1}1d_{5/2})$  and  $(1p_{3/2}^{-1}1d_{3/2})$  configurations.

Figure 6 shows the comparison between the experimental data and calculations performed with the code ANGCOR [47]. As seen in Fig. 6(a), the experimental data are well fitted with the assumption that the 7.7 MeV resonance has  $J^\pi=1^-$  with the  $(1p_{3/2}^{-1}1d_{5/2})$  configuration and excited with the substate population  $m=\pm 1$ .

The angular correlations of the decay protons from the  $2^-$  state with the two  $\Delta L=1$  configurations,  $(1p_{3/2}^{-1}2s_{1/2})$  and  $(1p_{3/2}^{-1}1d_{3/2})$  is flat. In the calculated correlation pattern for

TABLE II. Same as Table I, but for decay from the excitation-energy regions B–I to the 2.0 MeV  $\frac{1}{2}^-$  state and to the 4.3 and 4.8 MeV states in  $^{11}\text{C}$ .

Proton decay to the 2.0 MeV state in $^{11}\text{C}$			
Region	$A_0(\mu\text{b}/\text{sr}^2)$	$a_2$	$a_4$
B	$52.6 \pm 1.8$	$-0.20 \pm 0.08$	
	$55.5 \pm 3.3$	$-0.24 \pm 0.09$	$0.15 \pm 0.13$
C	$30.7 \pm 1.2$	$0.15 \pm 0.06$	
	$30.7 \pm 1.6$	$0.15 \pm 0.11$	$-0.00 \pm 0.10$
D	$34.3 \pm 0.6$	$0.50 \pm 0.04$	
	$34.5 \pm 0.7$	$0.04 \pm 0.04$	$0.07 \pm 0.07$
E	$37.3 \pm 1.4$	$0.24 \pm 0.09$	
	$37.1 \pm 2.0$	$0.25 \pm 0.12$	$-0.00 \pm 0.13$
F	$21.6 \pm 1.0$	$0.22 \pm 0.11$	
	$21.0 \pm 1.6$	$0.27 \pm 0.16$	$-0.00 \pm 0.17$
G	$17.5 \pm 0.6$	$0.29 \pm 0.12$	
	$15.6 \pm 1.1$	$0.05 \pm 0.17$	$-0.30 \pm 0.19$
H	$25.9 \pm 0.8$	$0.02 \pm 0.05$	
	$25.2 \pm 0.9$	$0.09 \pm 0.08$	$-0.10 \pm 0.12$
I	$10.3 \pm 0.5$	$-0.52 \pm 0.09$	
	$10.4 \pm 0.8$	$-0.54 \pm 0.11$	$0.04 \pm 0.19$
Proton decay to the 4.3 and 4.8 MeV states in $^{11}\text{C}$			
E	$61.3 \pm 0.9$	$-0.06 \pm 0.03$	
	$60.2 \pm 1.2$	$-0.02 \pm 0.04$	$-0.10 \pm 0.07$
F	$36.1 \pm 0.4$	$0.15 \pm 0.04$	
	$35.4 \pm 1.2$	$0.20 \pm 0.09$	$-0.00 \pm 0.10$
G	$33.9 \pm 0.7$	$0.25 \pm 0.04$	
	$33.3 \pm 0.8$	$0.29 \pm 0.05$	$-0.00 \pm 0.07$
H	$59.7 \pm 1.4$	$0.17 \pm 0.05$	
	$57.4 \pm 1.8$	$0.26 \pm 0.07$	$-0.10 \pm 0.08$
I	$27.2 \pm 0.4$	$-0.22 \pm 0.05$	
	$28.8 \pm 0.8$	$-0.24 \pm 0.05$	$0.20 \pm 0.08$

neutron decay of the  $2^-$  state with the  $(1p_{3/2}^{-1}1d_{5/2})$  configuration, maximum values appear at  $135^\circ$  and  $180^\circ$ . The observed angular correlation for the 7.7 MeV bump has clearly no maxima at these angles. Since the angular-correlation pattern monotonically changes with increasing neutron emission

TABLE III. Same as Table I, but for decay from the excitation-energy regions G–I to the 6.3 and 8.1 MeV states in  $^{11}\text{C}$ .

Proton decay to the 6.3 MeV state in $^{11}\text{C}$			
Region	$A_0(\mu\text{b}/\text{sr}^2)$	$a_2$	$a_4$
G	$11.7 \pm 1.4$	$-0.25 \pm 0.21$	
	$13.0 \pm 2.2$	$-0.37 \pm 0.22$	$0.27 \pm 0.30$
H	$23.0 \pm 4.7$	$0.25 \pm 0.41$	
	$23.4 \pm 5.9$	$0.21 \pm 0.55$	$0.06 \pm 0.53$
I	$9.9 \pm 0.5$	$0.20 \pm 0.10$	
	$8.5 \pm 0.9$	$0.59 \pm 0.27$	$-0.40 \pm 0.27$
Proton decay to the 8.1 MeV state in $^{11}\text{C}$			
G	$19.6 \pm 1.9$	$0.17 \pm 0.19$	
	$19.6 \pm 3.3$	$0.17 \pm 0.33$	$0.00 \pm 0.23$

angle, it would be difficult to fit the data with the  $2^-$  assumption for the 7.7 MeV resonance. Thus, the measurement of the neutron angular correlation favors the conclusion that the 7.7 MeV resonance has  $J^\pi=1^-$  with the  $(1p_{3/2}^{-1}1d_{5/2})$  configuration and is excited by spin flip.

## B. Structure of $^{12}\text{N}$

The strongly excited peak at  $E_x=4.1$  MeV in  $^{12}\text{N}$  has been observed in the  $^{12}\text{C}(^3\text{He},t)^{12}\text{N}$  reaction. This peak is known to be mainly due to the  $2^-$  state although a small peak due to the  $4^-$  state, which is actually excited with a weak intensity at  $\theta=0^\circ$  [15], could be present. The resonance region denoted by A ( $E_x=3.0$ – $5.0$  MeV) in Fig. 8 is further divided into two bins A1 ( $E_x=3.5$ – $4.5$  MeV) and A2 ( $E_x=4.5$ – $5.0$  MeV), and the angular correlations are obtained for each region. This binning is similar to that given in the previous  $(^3\text{He},t+p)$  work [26]. The obtained results are shown in Fig. 9 and listed in Table I. The present experiment shows that the angular correlations for proton decay from the subdivided regions A1 and A2 are not the same. In Ref. [26], it was also reported that the proton decay correlation patterns for the A1 and A2 regions differ from each other, and the difference could be explained by including some  $3^-$  or  $4^-$  excitation. In the present  $(^3\text{He},t)$  measurement at 450 MeV and  $\theta \approx 0^\circ$ , admixtures of the  $3^-$  and  $4^-$  states are expected to be small. This indicates that two levels of different structures contribute to the 4.1 MeV broad peak. This further may explain the fact that the observed width of 1.36 MeV in the present experiment is much larger than the 0.83 MeV width reported by Ref. [14] for the  $2^-$  state at 4.1 MeV. The angular correlation of decay protons from the 4.1 MeV resonance to the  $\frac{3}{2}^-$  ground state in  $^{11}\text{C}$  is well fitted by including the  $P_2(\cos\theta)$  term only. The  $P_4(\cos\theta)$  term is not needed in fitting the data although the coefficient  $a_4$  is, in principle, required in the case of  $J^\pi=2^-$  states.

In the regions B and C corresponding to the 7 MeV resonance in  $^{12}\text{N}$ , the angular-correlation patterns are essentially similar to those for the 4.1 MeV,  $2^-$  resonance decay to the  $\frac{3}{2}^-$ , ground state of  $^{11}\text{C}$ . Each fitted  $a_4$  coefficient for proton decay is significantly small, and the  $a_2$  coefficients are similar to those obtained by fitting the proton decay pattern from the 4.1 MeV region to the ground state. It should be noted that the proton-decay angular correlation from the excitation-energy region at  $\sim 7$  MeV in our  $^{12}\text{C}(^3\text{He},t+p)^{11}\text{C}$  experiment is clearly different from that of the neutron-decay correlation pattern in the  $^{12}\text{C}(d,^2\text{He}+n)^{11}\text{B}$  experiment; the proton-decay correlation pattern increases with increasing proton emission angle while that of neutron decay has an opposite behavior. If the substate population of the excited  $1^-$  states in the 7 MeV region in  $^{12}\text{N}$  differs from that of the  $(d,^2\text{He})$  reaction, or if the resonance observed in  $^{12}\text{N}$  includes several spin-flip and non-spin-flip states, then it may be possible to explain the observed difference (see below). At present, a model-independent conclusion to make a spin-parity assignment,  $J^\pi=1^-$  or  $2^-$ , for the 7 MeV resonance is not feasible on the basis of the experimental data alone.

The observed resonance at  $E_x \sim 7$  MeV in the  $^{12}\text{C}(^3\text{He},t)^{12}\text{N}$  singles spectrum (seen in Fig. 8) obviously consists of many peaks: there are many structures including a sharp state at 7.1 MeV. This suggests that in the 7 MeV

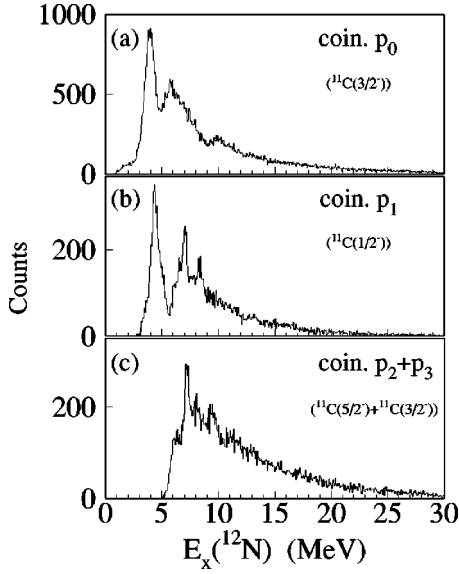


FIG. 14. Coincidence  $^{12}\text{C}(^3\text{He},t+p)$  spectra gated on proton decay to (a) the  $\frac{3}{2}^-$  ground state, to (b) the  $\frac{1}{2}^-$  state, and to (c) the  $\frac{5}{2}^-$ ,  $\frac{3}{2}^-$  states in  $^{11}\text{C}$ .

region, there are several states possibly consisting of  $1^-$  and  $2^-$  states and possibly other states with a mixture of spin-flip and non-spin-flip natures. This is consistent with the shell-model predictions [15]. Experimentally, it is difficult to extract the distributions of spin-flip and non-spin-flip strengths for the  $\Delta L=1$  transitions.

Figure 14 shows the coincidence spectra gated on proton decays to the  $1p_{3/2}^-$ ,  $\frac{3}{2}^-$  ground state, the first  $\frac{1}{2}^-$  state, and to the first  $\frac{5}{2}^-$  and second  $\frac{3}{2}^-$  states in  $^{11}\text{C}$ . One can clearly observe different populations from the intermediate resonances in  $^{12}\text{N}$  to these final states in  $^{11}\text{C}$ . The broad resonance at 4.1 MeV seems to split into two resonances: one decaying to the  $\frac{3}{2}^-$  ground state of  $^{11}\text{C}$  [Fig. 14(a)], and the higher one to the  $\frac{1}{2}^-$  first-excited state [Fig. 14(b)]. Considering that at these low decay energies for protons,  $l=0$  decay will be favored compared to  $l=2$  decay, since in the latter case, protons will have to penetrate both the Coulomb and centrifugal barriers, it appears that the lower resonance peak corresponds to a  $2^-$  state and the higher one to a  $1^-$  state.

This observation that two resonances may be involved in the 4.1 MeV bump is in agreement with the results from the angular correlations measured for regions A1 and A2, and is also consistent with the observation of the broader width in the present ( $^3\text{He},t$ ) measurement mentioned above.

The decay patterns from the 7 MeV resonance in  $^{12}\text{N}$  to the  $\frac{3}{2}^-$  ground state [Fig. 14(a)], the first  $\frac{1}{2}^-$  state [Fig. 14(b)], and to the first  $\frac{5}{2}^-$  and second  $\frac{3}{2}^-$  states [Fig. 14(c)] also differs from each other. A clear peak corresponding to the 6.4 MeV peak seen in region B in Fig. 8 is also identified in Fig. 14(a). However, the same peak disappears in Fig. 14(b). This suggests that the resonance at 6.4 MeV (denoted by region B in Fig. 8) mainly decays into the  $\frac{3}{2}^-$  ground state in  $^{11}\text{C}$ . On the other hand, the sharp peak at 7.1 MeV is not observed in the spectrum gated on proton decay to the  $\frac{3}{2}^-$  ground state in  $^{11}\text{C}$ . Instead, the 7.1 MeV state strongly populates the first  $\frac{1}{2}^-$  state, and the first  $\frac{5}{2}^-$  and second  $\frac{3}{2}^-$  states.

These observations on the proton-decay mode clearly indicate different microscopic structures for the two resonances at 6.4 and 7.1 MeV. When we put a gate on the 7.1 MeV resonance region in the ( $^3\text{He},t$ ) spectrum (corresponding to region C in Fig. 8), the ratio of proton decays to the  $\frac{3}{2}^-$ , g.s. and to the first  $\frac{1}{2}^-$  state is 1:0.48, whereas that obtained with a gate on the 6.4 MeV resonance region (corresponding to region B) is 1:0.25.

Anderson *et al.* predict three  $1_3^-$ ,  $1_4^-$ ,  $1_5^-$  states at 7.1, 7.8, and 8.5 MeV and two  $2_3^-$ ,  $2_4^-$  states at 6.1 and 6.8 MeV in the 7 MeV resonance region in  $^{12}\text{N}$ . They give the parentages for proton decay from the calculated  $1^-$  and  $2^-$  states to the low-lying neutron hole states in  $^{11}\text{C}$  [15]. We have estimated the proton transmission coefficients ( $T_p$ ) for these states using optical potentials and deduced the decay branches to the low-lying states in  $^{11}\text{C}$ . The results are given in Table IV together with the parentages ( $S_i$ ) given in Ref. [15]. By summing up  $\sum S_i T_p$  for each final state, we get the theoretical estimations for the branching ratios. The results are 1:0.1, 1:0.5, 1:0.0, 1:0.4, and 1:0.2 for the  $1_3^-$ ,  $1_4^-$ ,  $1_5^-$ ,  $2_3^-$ , and  $2_4^-$  states, respectively. If the 6.4 and 7.1 MeV resonances correspond to the  $1_3^-$  and  $1_4^-$  states, the observed branching ratios are rather consistent with the theoretical cal-

TABLE IV. Parentages ( $S_i$ ) and penetrabilities ( $T_p$ ) for proton decays from the states in the SDR region to the low-lying hole states in  $^{11}\text{C}$ . The parentages are taken from Table V in Ref. [15]. The branching ratios ( $R$ ) are obtained by summing up  $S_i \times T_p$  for each final state.

$E_x(^{12}\text{N})$	$1_3^-$			$1_4^-$			$1_5^-$			$2_3^-$			$2_4^-$		
	7.1 MeV			7.8 MeV			8.5 MeV			6.1 MeV			6.8 MeV		
	$S_i$	$T_p$	$R$												
$\frac{3}{2}^- \otimes s$	0.056	0.91	1.0 <sup>a</sup>	0.004	0.91	1.0 <sup>a</sup>	0.006	0.90	1.0 <sup>a</sup>	0.005	0.92	1.0 <sup>a</sup>	0.021	0.92	1.0 <sup>a</sup>
$\frac{3}{2}^- \otimes d$	0.579	0.73		0.289	0.78		0.158	0.81		0.446	0.64		0.275	0.71	
$\frac{1}{2}^- \otimes s$			0.1	0.057	0.92	0.5			0.0			0.4			0.2
$\frac{1}{2}^- \otimes d$	0.104	0.50		0.105	0.60		0.001	0.68		0.400	0.31		0.088	0.45	
$\frac{5}{2}^- \otimes s$			0.0			0.0			0.1	0.015	0.53	0.0	0.062	0.75	0.2
$\frac{5}{2}^- \otimes d$	0.127	0.09		0.030	0.20		0.027	0.33		0.042	0.01		0.010	0.06	
$\frac{3}{2}^- \otimes s$	0.048	0.77	0.1	0.097	0.85	0.6	0.61	0.89	4.2	0.021	0.42	0.0	0.310	0.71	1.1
$\frac{3}{2}^- \otimes d$	0.011	0.07		0.353	0.17		0.061	0.29		0.027	0.01		0.173	0.04	

<sup>a</sup>Normalized to 1.0.

culations. However, we cannot exclude the presence of the  $2_3^-$ , and  $2_4^-$  states in the 7 MeV region with a small probability, since these states are also expected to decay into the  $\frac{3}{2}_1^-$  and  $\frac{1}{2}_1^-$  states in  $^{11}\text{C}$  with comparable strengths. These arguments are obviously somewhat qualitative, since to arrive at good qualitative comparisons, the excitation probabilities of each state should be used to weight the branching ratios. This is imperative because the experimental results are obtained for regions in which different states with different cross sections and different branching ratios contribute.

As mentioned above, Sterrenburg *et al.* [26] reported the presence of a sharp state at  $E_x=7.63$  MeV in the  $^{12}\text{C}(^3\text{He},t)^{12}\text{N}$  reaction at  $E(^3\text{He})=81$  MeV and 75 MeV. They found that this state has strong proton decay into the  $\frac{5}{2}^-$  state in  $^{11}\text{C}$ . However, we could not find any evidence for such proton decays in the  $^{12}\text{C}(^3\text{He},t)^{12}\text{N}$  reaction at  $E(^3\text{He})=450$  MeV.

The angular correlations of proton decay from the  $7.9 < E_x(^{12}\text{N}) < 10.9$  MeV region (D and E regions in Fig. 8) to the ground state in  $^{11}\text{C}$  were well fitted by the  $P_2(\cos\theta)$  term. There is a sharp state at  $\sim 8.4$  MeV, which is clearly identified in both spectra gated on proton decays to the first  $\frac{1}{2}^-$  state and to the first  $\frac{5}{2}^-$  and  $\frac{3}{2}^-$  states in  $^{11}\text{C}$ . There is another peak observed at  $\sim 9.5$  MeV, which is rather broad ( $\Gamma \approx 0.7$  MeV) and observed only in the spectra gated on proton decays to the the first  $\frac{5}{2}^-$  and  $\frac{3}{2}^-$  states [see Fig. 14(c)].

In the theoretical calculation [44], a  $0^-$  state is predicted in the region of  $9.1 < E_x(^{12}\text{N}) < 10.9$  MeV (region E). Actually, we observed a clear bump at 9.9 MeV. If the bump corresponds to the  $0^-$  state, the angular correlation should be isotropic. Our experimental result shows that the angular-correlation pattern is not isotropic, but is similar to those for the 7 MeV resonance [see Figs. 9(d), 9(e), and 10(c)]. Thus, we cannot find any evidence for the presence of the  $0^-$  state in this excitation energy region. The resonance at 9.9 MeV strongly decays by proton emission into the  $\frac{3}{2}^-$  ground state in  $^{11}\text{C}$ . The bump is clearly observed in the spectrum gated with proton decays to the  $\frac{3}{2}^-$  ground state as shown in Fig. 14(a), but cannot be identified in Figs. 14(b) and 14(c).

We observed a small bump at 13.5 MeV on top of the nuclear continuum in the singles ( $^3\text{He},t$ ) reaction (region G in Fig. 8). The presence of this bump is not reported in the old ( $p,n$ ) experiments. In the coincidence spectra, the bump structure is fairly seen in Figs. 14(a) and 14(b). However, the presence of the resonance at 13.5 MeV is not evident.

The angular correlations of proton decays from regions E–F were fitted with Legendre polynomials. We found that the data can be well fitted with only the  $P_2(\cos\theta)$  term and the contribution of the  $P_4(\cos\theta)$  term is generally small.

## V. SUMMARY

The measurements of the ( $^3\text{He},t$ ) and ( $d,^2\text{He}$ ) reactions on  $^{12}\text{C}$  were performed to study the spin-isospin states in the mirror residual nuclei of  $^{12}\text{B}$  and  $^{12}\text{N}$ . We compared three spectra from the  $^{12}\text{C}(d,^2\text{He})$ ,  $^{12}\text{C}(\gamma,n)$ , and  $^{12}\text{C}(^3\text{He},t)$  reactions in view of their analog relation. Similar resonances populated with the  $\Delta L=1$  transferred momentum are found to exist in all the spectra. By comparing the  $^{12}\text{C}(^3\text{He},t)^{12}\text{N}$  and  $^{12}\text{C}(d,^2\text{He})^{12}\text{B}$  singles spectra at zero degrees, we ob-

serve a remarkable difference in the shape of the broad bumps corresponding to the spin-dipole resonances. This difference could be attributed to the different natures between the ( $d,^2\text{He}$ ) and ( $^3\text{He},t$ ) reactions; the former excites only  $\Delta S=1$  states and the latter excites both  $\Delta S=1$  and 0 states although at the present bombarding energy there is a strong preference for  $\Delta S=1$  states near zero degrees.

We succeeded to detect neutron decays from the excited states in  $^{12}\text{B}$  following the  $^{12}\text{C}(d,^2\text{He})^{12}\text{N}$  reaction using a triple coincidence method. This is an observation of direct neutron decay from spin-isospin resonances in  $^{12}\text{B}$ . The angular correlation for neutron decay from the 7.7 MeV bump in  $^{12}\text{B}$  to the ground state of  $^{11}\text{B}$  has been best fitted with the assumption that the 7.7 MeV resonance is mainly of  $1^-$  nature with a  $(1p_{3/2}^{-1}1d_{5/2})$  configuration.

Proton decays from  $^{12}\text{N}$  were also measured through the ( $^3\text{He},t$ ) reaction. In the case of the proton-decay measurement, we observed the decay branches from the excited states in  $^{12}\text{N}$  to the low-lying neutron-hole states in  $^{11}\text{C}$ . Through the study of the angular correlations of the 4.1 MeV broad peak, and its decay branching to the ground state and first-excited state in  $^{11}\text{C}$ , it was possible to infer that this broad peak is due to two resonances most probably having  $J^\pi=2^-$  and  $1^-$ , respectively, for the lower and higher resonance.

Contrary to the case of neutron decay, the angular correlation of the mirror proton decay from the 7 MeV resonance in  $^{12}\text{N}$  differs from that of the neutron decay. The branching ratio determined for decay to the  $\frac{3}{2}^-$  ground state and to the first  $\frac{1}{2}^-$  state in  $^{11}\text{C}$  was compared with the theoretical  $1p-1h$  calculations. We conclude that the 7 MeV resonance in  $^{12}\text{N}$  excited via the ( $^3\text{He},t$ ) reaction at 450 MeV consists of several different states, which are excited with similar strengths. The branching ratio indicates the presence of  $1^-$  states. But, we cannot exclude the contribution of  $2^-$  states. This makes it very difficult to try to fit the angular correlations model independently since each resonance can decay with more than one partial wave. In addition, the decay of the overlapping resonances will be adding coherently. These two points imply the necessity of a large number of free parameters to fit the angular correlations.

However, the present reliable experimental angular correlations and branching ratios give severe constraints on the various models used to predict the microscopic structure of the spin-isospin excitations in  $^{12}\text{B}$  and  $^{12}\text{N}$ . For example, in order to clarify the nature of the 7 MeV resonance, further theoretical analyses are in progress by combining the Tamm-Dancoff approximation to obtain the wave functions with the distorted-wave Born approximation code to get the excitation strengths and the decay branch calculations to get the branching ratios for decay into the final states in the residual nuclei [51].

## ACKNOWLEDGMENTS

The authors acknowledge the RCNP cyclotron staff for their support during the course of the present experiment. The present work was supported by the Ministry of Education, Science, Sports and Culture (Monbusho) with Grant No. 07404012. The present work was also supported in part by the Japan Society for the Promotion of Science (JSPS).

- [1] K. Ikeda, S. Fujii, and J. I. Fujita, *Phys. Lett.* **3**, 271 (1963).
- [2] J. I. Fujita and K. Ikeda, *Nucl. Phys.* **67**, 145 (1965).
- [3] D. E. Bainum, J. Rapaport, C. D. Goodman, D. J. Horen, C. C. Foster, M. B. Greenfield, and C. A. Goulding, *Phys. Rev. Lett.* **44**, 1751 (1980).
- [4] W. A. Sterrenburg, S. M. Austin, R. P. DeVito, and A. Galonsky, *Phys. Rev. Lett.* **45**, 1839 (1980).
- [5] D. J. Horen, C. D. Goodman, D. E. Bainum, C. C. Foster, C. Gaarde, C. A. Goulding, M. B. Greenfield, J. Rapaport, T. N. Taddeucci, E. Sugarbaker, T. Masterson, S. M. Austin, A. Galonsky, and W. A. Sterrenberg, *Phys. Lett.* **99B**, 383 (1981).
- [6] C. Gaarde, J. Rapaport, T. N. Taddeucci, C. D. Goodman, C. C. Foster, D. E. Bainum, C. A. Goulding, M. B. Greenfield, D. J. Horen, and E. Sugarbaker, *Nucl. Phys.* **A369**, 258 (1981).
- [7] A. Galonsky, J. P. Didelez, A. Djalois, and W. Oelert, *Phys. Lett.* **74B**, 176 (1978).
- [8] S. L. Tabor, C. C. Chang, M. T. Collins, G. J. Wagner, J. R. Wu, D. W. Halderson, and F. Petrovich, *Phys. Rev. C* **25**, 1253 (1982).
- [9] B. L. Berman and S. C. Fultz, *Rev. Mod. Phys.* **47**, 713 (1975).
- [10] H. Ejiri, K. Ikeda, and J. I. Fujita, *Phys. Rev.* **176**, 1277 (1968).
- [11] H. Ejiri and J. I. Fujita, *Phys. Rep., Phys. Lett.* **38C**, 85 (1978).
- [12] M. Ericson and J. Delorme, *Phys. Lett.* **67B**, 182 (1978); H. Toki and W. Weise, *Phys. Rev. Lett.* **42**, 1034 (1979); J. Meyer-Ter-Vehn, *Phys. Rev. C* **24**, 323 (1981); E. Oset, H. Toki, and W. Weise, *Phys. Rep.* **83**, 281 (1982); G. E. Brown and M. Rho, *Nucl. Phys.* **A372**, 397 (1981); K. Kubodera, J. Delorme, and M. Rho, *Phys. Rev. Lett.* **40**, 755 (1978).
- [13] R. Madey, B. S. Flanders, B. D. Anderson, A. R. Baldwin, W. Bertozzi, T. Chritrakarn, J. R. Comfort, J. M. Finn, C. C. Foster, C. Hyde-Wright, J. J. Kelly, C. Lebo, H. Orihara, W. Pairsuwan, and J. W. Watson, *Phys. Rev. C* **56**, 3210 (1997).
- [14] F. Ajzenberg-Selove, *Nucl. Phys.* **A506**, 1 (1990).
- [15] B. D. Anderson, L. A. C. Garcia, D. J. Millener, D. M. Manley, A. R. Baldwin, A. Fazely, R. Madey, N. Tamimi, J. W. Watson, and C. C. Foster, *Phys. Rev. C* **54**, 237 (1996).
- [16] X. Yang, L. Wang, J. Rapaport, C. D. Goodman, C. C. Foster, Y. Wang, E. Sugarbaker, D. Marchlinski, S. de Lucia, B. Luther, L. Rybarczyk, T. N. Taddeucci, and B. K. Park, *Phys. Rev. C* **52**, 2535 (1995).
- [17] H. Okamura, S. Ishida, N. Sakamoto, H. Otsu, T. Uesaka, T. Wakasa, Y. Satoh, T. Fujita, H. Sakai, T. Niizeki, K. Katoh, T. Yamamoto, T. Yamashita, Y. Hara, H. Ohnuma, T. Ichihara, and K. Hatanaka, *Nucl. Phys.* **A577**, 89c (1994).
- [18] H. Okamura, S. Fujita, Y. Hara, K. Hatanaka, T. Ichihara, S. Ishida, K. Katoh, T. Niizeki, H. Ohnuma, H. Otsu, H. Sakai, N. Sakamoto, Y. Satou, T. Uesaka, T. Wakasa, and T. Yamashita, *Phys. Lett. B* **345**, 1 (1995).
- [19] K. Nagatani, *Phys. Lett.* **27B**, 187 (1968).
- [20] H. Ohnuma, K. Hatanaka, S. I. Hayakawa, M. Hosaka, T. Ichihara, S. Ishida, S. Kato, T. Niizeki, M. Ohura, H. Okamura, H. Orihara, H. Sakai, H. Shimizu, Y. Tajima, H. Toyokawa, H. Y. Yoshida, and M. Yosoi, *Phys. Rev. C* **47**, 648 (1993).
- [21] T. Niizeki, H. Ohnuma, T. Yamamoto, K. Katoh, T. Yamashita, Y. Hara, H. Okamura, H. Sakai, S. Ishida, N. Sakamoto, H. Otsu, T. Wakasa, T. Uesaka, Y. Satou, T. Fujita, T. Ichihara, H. Orihara, H. Toyokawa, K. Hatanaka, S. Kato, S. Kubuno, and M. Yosoi, *Nucl. Phys.* **A577**, 37c (1994).
- [22] H. M. Xu, G. K. Ajupova, A. C. Betker, C. A. Gagliardi, B. Kokenge, Y.-W. Lui, and A. F. Zaruba, *Phys. Rev. C* **52**, 1161 (1995).
- [23] S. Nakayama, T. Yamagata, K. Yuasa, M. Tanaka, M. Inoue, T. Itahashi, and H. Ogata, *Phys. Rev. C* **34**, 366 (1986).
- [24] S. Nakayama, T. Yamagata, M. Tanaka, M. Inoue, K. Yuasa, T. Itahashi, H. Ogata, N. Koori, and K. Shima, *Phys. Rev. Lett.* **67**, 1082 (1991).
- [25] S. Nakayama, T. Yamagata, M. Tanaka, M. Inoue, K. Yuasa, T. Itahashi, H. Ogata, N. Koori, K. Shima, and M. G. Greenfield, *Phys. Rev. C* **46**, 1667 (1992).
- [26] W. A. Sterrenburg, M. N. Harakeh, S. Y. van der Werf, and A. van der Woude, *Nucl. Phys.* **A405**, 109 (1983).
- [27] W. A. Sterrenburg, S. Brandenburg, J. H. van Dijk, A. G. Drentje, M. B. Greenfield, M. N. Harakeh, H. Riezboos, H. Sakai, W. Segeth, S. Y. van der Werf, and A. van der Woude, *Nucl. Phys.* **A420**, 257 (1984).
- [28] M. Fujiwara, H. Akimune, I. Daito, H. Ejiri, Y. Fujita, M. B. Greenfield, M. N. Harakeh, T. Inomata, J. Jänecke, S. Nakayama, N. Takemura, A. Tamii, M. Tanaka, H. Toyokawa, and M. Yosoi, *Nucl. Phys.* **A599**, 223c (1996).
- [29] H. Akimune, I. Daito, Y. Fujita, M. Fujiwara, M. B. Greenfield, M. N. Harekeh, T. Inomata, J. Jänecke, K. Katori, S. Nakayama, H. Sakai, Y. Sakemi, M. Tanaka, and M. Yosoi, *Nucl. Phys.* **A569**, 245c (1994).
- [30] M. Fujiwara, H. Akimune, I. Daito, H. Ejiri, Y. Fujita, M. B. Greenfield, M. N. Harakeh, R. Hazama, T. Inomata, J. Jänecke, N. Kudomi, K. Kume, S. Nakayama, K. Shinmyo, A. Tamii, M. Tanaka, H. Toyokawa, and M. Yosoi, *Nucl. Phys.* **A577**, 43c (1994).
- [31] Y. Fujita, M. Fujiwara, H. Akimune, I. Daito, M. B. Greenfield, M. N. Harekeh, T. Inomata, J. Jänecke, K. Katori, H. Nakada, S. Nakayama, H. Sakai, Y. Sakemi, M. Tanaka, H. Toyokawa, and M. Yosoi, *Phys. Lett. B* **365**, 29 (1996).
- [32] M. N. Harekeh, H. Akimune, I. Daito, Y. Fujita, M. Fujiwara, M. B. Greenfield, T. Inomata, J. Jänecke, K. Katori, S. Nakayama, H. Sakai, Y. Sakemi, M. Tanaka, and M. Yosoi, *Nucl. Phys.* **A577**, 57c (1994).
- [33] H. Akimune, I. Daito, Y. Fujita, M. Fujiwara, M. B. Greenfield, M. N. Harakeh, T. Inomata, J. Jänecke, K. Katori, S. Nakayama, H. Sakai, Y. Sakemi, M. Tanaka, and M. Yosoi, *Phys. Lett. B* **323**, 107 (1994).
- [34] H. Akimune, I. Daito, Y. Fujita, M. Fujiwara, M. B. Greenfield, M. N. Harakeh, T. Inomata, J. Jänecke, K. Katori, S. Nakayama, H. Sakai, Y. Sakemi, M. Tanaka, and M. Yosoi, *Phys. Rev. C* **52**, 604 (1995).
- [35] N. Matsuoka, T. Noro, K. Sagara, S. Morinobu, and K. Hatanaka, *RCNP Annual Report*, p. 186 (1991).
- [36] H. Laurent, H. Lefort, D. Beaumel, Y. Blumenfeld, S. Fortier, S. Gales, J. Guillot, J. C. Roynette, P. Volkov, and S. Brandenburg, *Nucl. Instrum. Methods Phys. Res. A* **326**, 517 (1993).
- [37] V. V. Verbinski, W. R. Burrus, T. A. Love, W. Zobel, and N. W. Hill, *Nucl. Instrum. Methods* **65**, 8 (1968).
- [38] M. Fujiwara, in *Proceedings of the 5th French-Japanese Symposium on Nuclear Physics, Dogashima, Japan, 1989*, p. 348; M. Fujiwara, S. Morinobu, M. Yosoi, and H. Ikegami, in *Proceedings of the International Symposium on Heavy Ion Research with Magnetic Spectrographs* (MSU, East Lansing, 1989), p. 283; M. Fujiwara, *Ionics* **20**, 113 (1994) (Japanese).
- [39] K. Dennis, H. Akimune, G. P. A. Berg, S. Chang, B. Davis, M. Fujiwara, M. N. Harakeh, J. Jänecke, J. Lin, K. Pham, D. A.

- Robert, and E. J. Stephenson, *Phys. Rev. A* **50**, 3992 (1994).
- [40] M. Matsuoka, T. Noro, K. Tamura, M. Yoshimura, M. Yosoi, A. Okihana, and M. Yoshimura, *Phys. Lett. B* **359**, 39 (1995).
- [41] I. Bergqvist, A. Brockstedt, L. Carlén, L. P. Ekström, B. Jakobsson, C. Ellegaard, C. Gaarde, J. S. Larsen, C. Goodman, M. Bedjidian, D. Contardo, J. Y. Grossiord, A. Guichard, R. Haroutunian, J. R. Pizzi, D. Bachelier, J. L. Boyard, T. Hennino, J. C. Jourdain, M. Roy-Stephan, M. Boivin, and P. Radvanyi, *Nucl. Phys. A* **469**, 648 (1987).
- [42] W. G. Love and M. A. Franey, *Phys. Rev. C* **24**, 1073 (1981).
- [43] F. Osterfeld, *Rev. Mod. Phys.* **64**, 491 (1992).
- [44] V. Gillet and N. Vinh Mau, *Nucl. Phys.* **54**, 321 (1964).
- [45] F. P. Brady, T. D. Ford, G. A. Neadham, J. L. Romero, D. S. Sorenson, C. M. Casteneda, J. L. Drummond, E. L. Hjort, B. McEachern, N. S. P. King, and D. J. Millener, *Phys. Rev. C* **43**, 2284 (1991).
- [46] R. S. Hicks, J. B. Flanz, R. A. Lindgren, G. A. Peterson, L. W. Fagg, and D. J. Millener, *Phys. Rev. C* **30**, 1 (1984).
- [47] M. N. Harakeh and L. W. Put, KVI internal report, KVI 67 (1979).
- [48] T. Ichihara, M. Ishihara, H. Ohnuma, T. Niizeki, T. Yamamoto, K. Katoh, T. Yamaashita, Y. Fuchi, S. Kubono, M. H. Tanaka, H. Okamura, S. Ishida, and T. Uesaka, *Nucl. Phys. A* **577**, 93c (1994).
- [49] C. Gaarde, J. S. Larsen, H. Sagawa, N. Ohtsuka, J. Rapaport, T. N. Taddeucci, C. D. Goodman, C. C. Foster, C. A. Goulding, D. J. Horen, T. Masterson, and E. Sugerbaker, *Nucl. Phys. A* **422**, 189 (1984).
- [50] X. Yang, L. Wang, and J. Rapaport, *Phys. Rev. C* **48**, 1158 (1993).
- [51] B. K. Kim and T. Udagawa, *Nucl. Instrum. Methods Phys. Res. A* **402**, 354 (1998).